Available online at www.sciencedirect.com

ScienceDirect

Advances in Space Research 60 (2017) 153–165

ADVANCES IN SPACE RESEARCH (a COSPAR publication)

www.elsevier.com/locate/asr

Probing interferometric parallax with interplanetary spacecraft

G. Rodeghiero [a,b,*], F. Gini [c], N. Marchili [a], P. Jain [d], J.P. Ralston [e], D. Dallacasa [f], G. Naletto [g], A. Possenti [h], C. Barbieri [a], A. Franceschini [a], L. Zampieri [i]

[a] Department of Physics and Astronomy, University of Padova, Italy
[b] Max Planck Institut für Astronomie, Königstuhl 17, D-69117 Heidelberg, Germany
[c] ESOC, Robert-Bosch-Straße 5, 64293 Darmstadt, Germany
[d] Physics Department, IIT, Kanpur 208016, India
[e] Department of Physics and Astronomy, University of Kansas, Lawrence, KS 66045, USA
[f] Istituto di Radioastronomia of INAF, 40129 BO, Italy
[g] Department of Information Engineering, University of Padova, Italy
[h] Cagliari Astronomical Observatory, Italy
[i] INAF Astronomical Observatory of Padova, Italy

Received 8 December 2015; received in revised form 12 February 2017; accepted 26 March 2017
Available online 31 March 2017

Abstract

We describe an experimental scenario for testing a novel method to measure distance and proper motion of astronomical sources. The method is based on multi-epoch observations of amplitude or intensity correlations between separate receiving systems. This technique is called Interferometric Parallax, and efficiently exploits phase information that has traditionally been overlooked. The test case we discuss combines amplitude correlations of signals from deep space interplanetary spacecraft with those from distant galactic and extragalactic radio sources with the goal of estimating the interplanetary spacecraft distance. Interferometric parallax relies on the detection of wavefront curvature effects in signals collected by pairs of separate receiving systems. The method shows promising potentialities over current techniques when the target is unresolved from the background reference sources. Developments in this field might lead to the construction of an independent, geometrical cosmic distance ladder using a dedicated project and future generation instruments. We present a conceptual overview supported by numerical estimates of its performances applied to a spacecraft orbiting the Solar System. Simulations support the feasibility of measurements with a simple and time-saving observational scheme using current facilities.

Keywords: Distance; Interferometric parallax phase; Interferometry; Spacecraft

1. Introduction

The direct estimate of distances in Astronomy has always been one of the most difficult measurements to perform. Although many indirect methods based on photometric and spectroscopic observations already exist, the methods providing direct, geometric distance of the celestial bodies, independent of any additional parameter, is limited to our own Galaxy. At optical wavelengths, the method of the trigonometric parallax (TP) probed distances to the order of kpc with the Hipparcos satellite for more than 100.000 stars in the solar neighborhood (Perryman et al., 1997) and the GAIA mission aims to extend this measurement to ~1 billion stars (de Bruijne, 2012). At radio frequencies, examples of TP measurement are provided by Hachisuka et al. (2006), Reid et al. (2009) and van Langevelde et al. (1999) that estimated the distances and proper motions of galactic masers by

* Corresponding author at: Max Planck Institut für Astronomie, Königstuhl 17, D-69117 Heidelberg, Germany.
E-mail address: rodeghiero@mpia.de (G. Rodeghiero).

http://dx.doi.org/10.1016/j.asr.2017.03.038
0273-1177/

means of the Very Long Baseline Array (VLBA) and Japanese Very Long Baseline Interferometry (VLBI), exploring the nearby interstellar medium until ~10 kpc. However the TP technique requires extreme instrumental stability to produce images of the quality to obtain precise astrometric analyses.

A new method to estimate distances and proper motions called *interferometric parallax* (IP) has been proposed by Jain and Ralston (2008). This method differs substantially from TP and it does not require a precise measurement of the object's angular position, neither by making an image nor resolving the object under study. The IP method entirely bypasses the step of image production/acquisition, while concentrating on the raw signals collected by pairs of receivers. The measurements can be performed either with the amplitude interferometry at radio frequencies or by using the optical intensity interferometry, subject of revived interest thanks to the upcoming Cherenkov Telescope Array (CTA) (Dravins et al., 2012).

While interferometers work in the Fraunhofer far field hypothesis, IP relies on an extension of the Van Cittert-Zernike (VCZ) theorem that assumes a plane wave approximation. The extension includes effects from the curvature of the wavefronts from a source at finite distance, which contributes an observable phase difference. The basic use of IP assumes the observation of a foreground object (target) and one background object (reference) that are angularly close and point-like sources; by studying the equal time correlated signals retrieved from a pair of separate receivers as a function of time over a suitable period that ranges from days up to six months, the distance of the foreground object is measured.

As a pathfinder experiment for IP verification we seek to measure the distance of an object orbiting the Solar System and producing a fairly detectable IP effect over a short time period. The test case we describe exploits amplitude correlations of signals from deep space spacecraft in conjunction with distant galactic and extragalactic radio sources (Fig. 1). The target bodies envisaged for this pilot experiment are Cassini, Juno, Dawn and New Horizons spacecraft. VLBA astrometric observations of the Cassini spacecraft were carried out by Jones et al. (2011) to improve the Saturn planetary ephemerides. The Cassini spacecraft was used as a bright artificial radio source and its precise astrometry was retrieved. We suggest to observe spacecraft signals with a similar approach that includes significant new features, to estimate the average distance and proper motion coordinates of the spacecraft at some suitable times when we can conveniently extract the parallax phase.

Once the reliability of the method is assessed within the Solar System scale, a direct cosmic distance ladder could be established by comparing objects at progressively greater distances provided that a dedicated project and future technological developments will be achieved. In this perspective, the amplitude correlations between wavefronts from a galactic maser or a pulsar and those of a radio galaxy can be studied to probe a galaxy-size distance scale. In the case of intensity interferometry (II), the distances that could be probed are limited at a galactic scale due to the intrinsic lower signal to noise ratio of this observation mode. Although with this limitation, II could lead to measure the distance of foreground galactic stars angularly close to stellar objects belonging to a background star cluster, or vice versa, i.e. when a member of a foreground star cluster is angularly close to a background star field. In addition, the galactic stars distance could be measured exploiting a transient bright background object as a nova or a supernova. The existence of wave curvature corrections has been recognized in precise VLBI time delays calculation within the Solar System (Kopeikin and Schäfer, 1999). The novelty of the proposed approach consists in detecting this corrective term by interferometry, and then using it as a tool for direct distance and proper motion estimation overcoming the limitations of image-based analysis.

In this paper the mathematical derivation of the method and the differences between the trigonometric parallax are first described (Section 2). Then the motivation for the use of a spacecraft for the verification of the technique is presented (Section 3). The simulations on the observing scenario and the technical aspects of the observations are discussed in Section 4. Finally, the possible applications to the observation of some astrophysical sources and the perspectives with the next generation of ground-based large telescopes are briefly presented.

2. Experimental overview

The method requires a source nearby (the spacecraft) and a very distant astronomical source (the background radio source). Fig. 1 shows the orbit of Cassini projected on the sky plane along with a number of background radio sources for the year 2016. The simulation can be easily extended to any epoch of interest. There are many near conjunctions of Cassini with the radio sources in the NRAO VLA Sky Survey (NVSS) (Condon et al., 1998). These radio sources are our reference objects for the interferometric parallax measurement. As we will show, each radio source provides an independent opportunity for the direct determination of the distance between the telescope receiver and the spacecraft. The Cassini spacecraft is assumed as an example candidate, but the derivation is valid for all other spacecraft in general. The description of the method and the mathematics reported in Sections 2.1 and 2.2 are entirely based on the formalisms assumed and used in Jain and Ralston (2008).

2.1. Background and definitions

Consider an array of two receivers, labeled 1 and 2, with vector coordinates $\mathbf{x}_1$ and $\mathbf{x}_2$ relative to a given origin. It will be convenient to represent the coordinates in terms of their separation $\Delta\mathbf{x}_{12} = \mathbf{x}_2 - \mathbf{x}_1$ and a center of mass vector $\mathbf{X}_{12} = (\mathbf{x}_1 + \mathbf{x}_2)/2$. Each receiver observes the signal

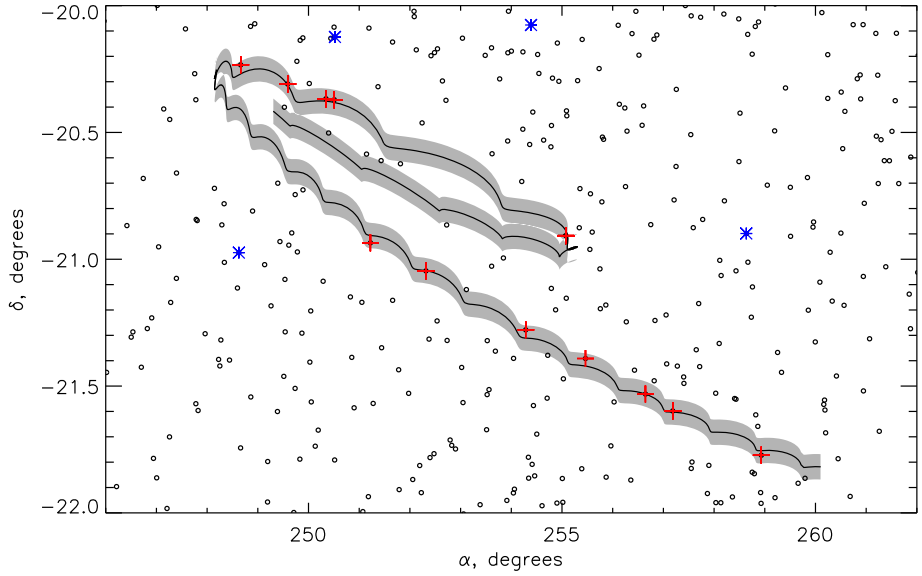

Fig. 1. The Cassini epicyclic trajectory over 2016 (easily extensible to any epoch) calculated by the NASA Horizons System (Nasa website for spacecraft ephemerides) powered by JPL as seen from a mid latitude Earth site (e.g. VLA Observatory). The field of view in X band ($\lambda = 3.6$ cm) of a 25 m antenna ($\sim 6'$) is represented by the shaded area around the Cassini orbit. The NVSS sources above a flux density $F = 0.01$ Jy are represented by the gray circles. NVSS sources angularly close to Cassini and well-suited for the IP measurement are represented by red crosses. The blue asterisks represent the calibrators ($F > 200$ mJy) from the VLBA Calibrators List provided by NRAO for phase referencing available in the field.

from two unresolved objects located at a very small angular separation, but at very different distances to the Earth: the close object is the spacecraft, while the distant one is a natural background radio source. The location of these two sources in the reference frame of the array receivers is parametrized by $\mathbf{r}$ and $\mathbf{r}'$ that represent the observer-source vector. A schematics of the observation is shown in Fig. 2. If the pair is unresolved from the antenna, each receiver responds to the total field $E = E_{spacecraft} + E_{radiosource}$. The correlation of a given frequency and polarization of electric fields measured in the receivers is denoted $\langle E(x_1)E^*(x_2)\rangle$, and given by:

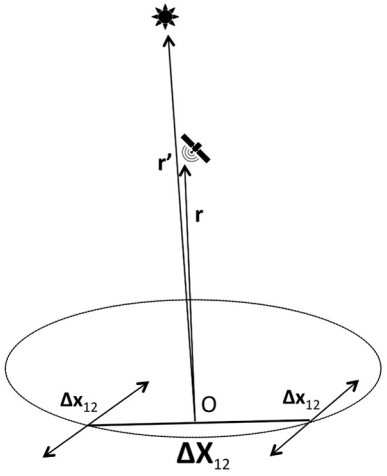

Fig. 2. Schematics of the IP observation: the array baseline is $\Delta\mathbf{x}_{12}$ and the orbital baseline is $\Delta\mathbf{X}_{12}$. $\mathbf{r}$ and $\mathbf{r}'$ are the position vectors of the two sources, the target and reference relative to a given origin $\mathbf{O}$ that can arbitrarily be in the vicinity of the receivers.

$$\langle E_1 E_2^* \rangle = e^{-ik\psi}\left[\frac{I_S}{\mathbf{r}^2} + \frac{I'_S}{\mathbf{r}'^2} e^{-i\phi_{12}^{tot}}\right] \tag{1}$$

where I_S and $I_{S'}$ parameterize the source intensities from the two objects respectively. The relative phase ϕ_{12}^{tot} between the two receivers contains information on the separation of the two sources. Let ϕ_{12}^0 represent the *plane wave approximation* to the total phase caused by receivers-sources orientation:

$$\phi_{12}^0 = k\Delta\mathbf{x}_{12} \cdot (\hat{\mathbf{r}} - \hat{\mathbf{r}}') \tag{2}$$

where $\hat{\mathbf{r}}, \hat{\mathbf{r}}'$ are the unit vectors pointing to the sources, located at vectors $\mathbf{r}$ and $\mathbf{r}'$, and $k = 2\pi/\lambda$ is the wavenumber. This is the prediction of the standard Van Cittert-Zernike (VCZ) theorem, and ϕ_{12}^0 can be called the zeroth-order or VCZ phase. Note that ϕ_{12}^0 represents the geometric phase contribution between two elements of an array (as extensively discussed in Section 4.1). Here we are treating the two sources as idealized point sources and hence only the difference $(\hat{\mathbf{r}} - \hat{\mathbf{r}}')$ appears in this phase. Finite source size effects are discussed in Jain and Ralston (2008). The plane wave approximation puts all the sources at an infinite distance. Conversely, when the source is at finite distance, its wavefronts are curved. The curvature produces an additional phase shift, called $\phi_{12}^{parallax}$, from which $\phi_{12}^{tot} = \phi_{12}^0 + \phi_{12}^{parallax}$, where

$$\phi_{12}^{parallax} = -k\left(\frac{1}{r} - \frac{1}{r'}\right)\Delta\mathbf{x}_{12} \cdot \delta_T \cdot \mathbf{X}_{12} \tag{3}$$

The symbol $\delta_T \to \delta(r)_T^{ij} = \delta^{ij} - \hat{r}^i\hat{r}^j$ is a projector that removes the vector components parallel to $\hat{r}$, retaining

the components in the plane of the sky unchanged. The formula comes from expanding the phase differences to the next order of approximation and re-computing the correlations (see Appendix A for details). Note that Eq. (3) is dependent on the distance between the receivers and the source. The $1/r$ dependence of the *parallax phase* is similar to the $1/r$ dependence of image offsets in TP measurements. No image needs to be made, instead the method entirely relies on the direct measurement of the parallax phase using the interferometry. Eq. (1) also contains an overall phase ψ. Calculation to the same order of approximation as above gives

$$\psi = \hat{\mathbf{r}} \cdot (\mathbf{x}_1 - \mathbf{x}_2) - \sum_{i,j=1}^{3} \left(x_1^i x_1^j - x_2^i x_2^j\right) \delta_T^{ij}(\mathbf{r})/2r \tag{4}$$

Our approach concentrates on the phase changes observable over the course of the experiment.

2.2. Translational dependence

The dependence of the interference pattern on the array center of mass position $\mathbf{X}_{12}$ is absent in the plane wave approximation: plane waves are unchanged by translations of the observer parallel to the wave plane. However, when the foreground source is at finite distance, its wavefronts are curved and the correlations depend on the relative motion of the receivers and sources. Following (Jain and Ralston, 2008), we consider the case where the sources are fixed in space and the detectors are moving. The receivers are translated across wavefronts of the "fixed in space" distant sources with slightly different curvature. The translation vector of the center of mass vector $\mathbf{\Delta X}_{12}$ originates from the Earth revolution motion around the Sun, while the projection of the relative position vector between the two receivers $\Delta\mathbf{x}_{12}$ changes its direction and modulus due to the Earth's rotation. After a net translation $\mathbf{X}_{12} \rightarrow \mathbf{X}_{12} + \Delta\mathbf{X}_{12}$, the relative phase between the two receivers (neglecting the Earth's rotation for this discussion) will be:

$$\phi_{12}^0 \rightarrow \phi_{12}^0$$

$$\phi_{12}^{parallax} \rightarrow \phi_{12}^{parallax} + \Delta\phi_{12}^{parallax}$$

The phase of the signal contains a quasi-constant term ϕ_{12}^0 and a linearly growing term proportional to the translation vector $\Delta\mathbf{X}_{12}$:

$$\Delta\phi_{12}^{parallax} = -k\left(\frac{1}{r} - \frac{1}{r'}\right)\Delta\mathbf{x}_{12} \cdot \delta_T \cdot \Delta\mathbf{X}_{12} \tag{5}$$

Working with two different phases explicitly isolates the distance coordinate in the parallax phase while keeping the dependence on the angular separation of the pair in ϕ_{12}^0. Hence, observationally the term $(\hat{r} - \hat{r}')$ should be interpreted as the mean difference between these two unit vectors over the range of observations and does not have any dependence on r and time. Alternatively we may choose not to make the expansion in powers of $1/r$. In this case the contribution due to the parallax term is implicitly contained in ϕ_{12}^0 which now changes at a rate proportional to $1/r$. The greater the array baseline $\Delta\mathbf{x}_{12}$ and the translation vector $\Delta\mathbf{X}_{12}$, the larger the parallax phase, up to the point where series approximations used in the formula break down.[1] $\Delta\mathbf{X}_{12}$ can be regarded as a sort of *orbital baseline*. Assuming the distant source is effectively at infinity ($1/r' \rightarrow 0$), a measurement of the relative parallax phase leads to a direct distance determination of the foreground object:

$$r \sim \frac{\Delta X \Delta x}{\Delta\phi_{12}^{parallax}\lambda} \tag{6}$$

The quantities Δx and ΔX are the projection in the $u - v$ plane (plane normal to the direction of photon propagation) of the ground and orbital baselines $\Delta\mathbf{x}_{12}$ and $\Delta\mathbf{X}_{12}$. The latter are computed using planetary ephemerides and array geometry, the former by accurate simulations of the projected components. The phase difference $\Delta\phi_{12}^{parallax}$ is the observable to be retrieved by the experiment. A source at infinity is required as a reference-flat wavefront emitter that emits random fluctuations totally independent from the target fluctuations. The detection of a certain coincidence between the background source and the target fluctuations depends on the relative orientation of the sources and receivers, the array baseline, and the source distances. As the orbital baseline changes, the flat wavefronts from the background source remain unchanged while those curved wavefronts emitted by the foreground object vary the phase and correlations of the overall signal $(E_{spacecraft} + E_{radiosource})$. We discuss this in more detail below.

2.3. Advantages and requirements of the interferometric parallax

As discussed in Section 2.1 the interferometric parallax method requires (i) measuring the equal time correlations from two angularly close sources with two or more receivers, then (ii) repeating the measurement after the array is translated, and finally (iii) extracting a relative phase by comparing the two observations from different epochs. The relative magnitude of the parallax effect is very small in most cosmological circumstances. With suitable technology development we might contemplate a measurement to 100 kpc as shown in the following. The main complication comes from the size of the VCZ phase ϕ_{12}^0 compared to parallax phase $\phi_{12}^{parallax}$. From Eqs. (7) and (8) the order of magnitudes are

$$\phi_{12}^0 \sim 10^4 \text{ rad}\left(\frac{\Delta\theta}{\text{arcsec}}\right)\left(\frac{1\text{ cm}}{\lambda}\right)\left(\frac{\Delta x_{12}}{10^4\text{ km}}\right) \tag{7}$$

[1] The series expansions are always consistent whenever the parallax phase is small compared to the VCZ phase.

$$\phi_{12}^{parallax} \sim 10^{-1}\ \text{rad}\left(\frac{\Delta X_{12}}{\text{AU}}\right)\left(\frac{100\ \text{kpc}}{r}\right)\left(\frac{1\ \text{cm}}{\lambda}\right)\left(\frac{\Delta x_{12}}{10^4\ \text{km}}\right) \quad (8)$$

The second equation shows that $\phi_{12}^{parallax}$ is not itself intrinsically small for the parameters used: it is simply small compared to the other phase. At radio frequencies (e.g. $\lambda = 1$ cm) and using $\Delta X_{12} \sim AU$ the ratio of the two phase terms is about 10^{-5} for sources separated by arc-second values at distances $r \sim 100$ kpc. The fact that, at 1 cm wavelength, $\phi_{12}^{parallax} \sim 0.1$ rad, indicates that measurements out to that distance are at least in principle possible with dedicated, future hardware solutions. The relative size of the parallax term is maximized by pushing the translation vector $\Delta\mathbf{X}_{12}$ toward ~ 1 AU and by selecting a very close pair of objects (minimizing $\Delta\theta$). In such circumstances the ratio of $\phi_{12}^{parallax}$ over ϕ_{12}^{0} can be significant. In this scenario, the pair might be unresolved by standard imaging technique and TP completely prevented, while IP could be used to provide distance information. If the pair separation is large and the phase ratio is disfavored, the limitation may be overcome if the observation is carried out under two different baselines with nearly the same length, as reported in Jain and Ralston (2008, Section 2.5). The technique is called *4-points correlation* in the original paper and it leads to a correlation expression, in principle free from VCZ phase dependence. Furthermore, there is a special alignment of the interferometric baseline relative to the orientation of the source, which minimizes the error in the measurement of the VCZ phase (Jain and Ralston, 2008, Appendix A.2). From Eqs. (7) and (8) one deduces that $\phi_{12}^{parallax}$ and ϕ_{12}^{0} have different behavior and dependence on the pair angular separation and the orbital baseline as shown in Figs. 3 and 4. The phase ϕ_{12}^{0} while remaining constant with the orbital baseline ΔX_{12} it increases proportionally to the pair separation. In contrast, $\phi^{parallax}$ has exactly

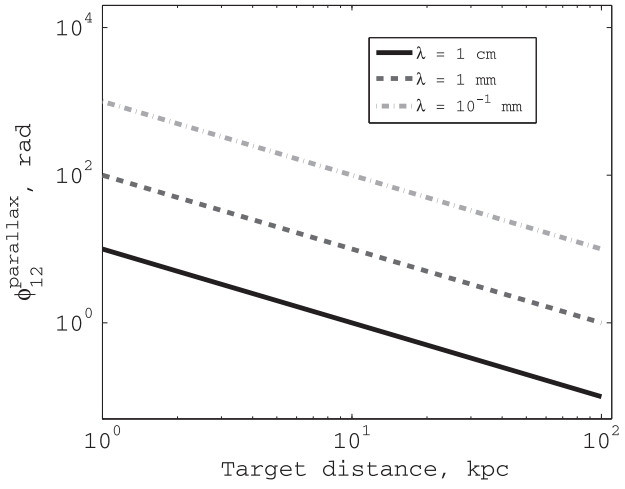

Fig. 3. The interferometric parallax phase $\phi_{12}^{parallax}$ is inversely proportional to the target distance. Both $\phi_{12}^{parallax}$ and ϕ_{12}^{0} increase for progressively smaller wavelengths. (Logarithmic scale.)

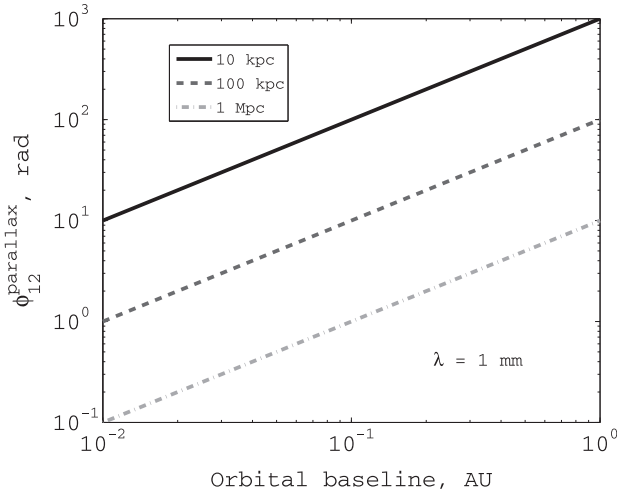

Fig. 4. Interferometric parallax phase $\phi_{12}^{parallax}$ estimation for different target object distances for a wavelength $\lambda = 1$ mm. The parameter space below the 10 kpc line has never been probed through direct distance estimation methods. (Logarithmic scale.)

the opposite behavior: it does not depend on the angular separation of the pair while it grows proportionally to the orbital baseline.

The above considerations point to some cons and pros of IP compared to the classical TP method:

- TP requires accurate measurement of the object angular position either by centroid or point spread function fitting and it is limited by the image quality and system resolution. The finest measurements based on these methods generally achieves hundredths of pixel accuracy. IP has the great advantage over TP of working also for unresolved pair (target + reference). Both the methods rely on the finite distance of the object under study to estimate its radial coordinate from the observer, but while TP uses fine image analyses to measure the angular shift of the target with respect to a reference source, IP relies on interferometry to measure a phase shift in the interference pattern and measures directly the curvature effects down to a resolution $\sim \lambda/(\Delta x \Delta X)$. Measuring the wavefront curvature by tracking a fringe function shift (at radio wavelengths) or a variation in photons times of arrival (at optical wavelengths) may provide distance measurements also for unresolved pair of objects that are unobservable with TP.
- IP suffers the same limitation of the trigonometric parallax of having distance and proper motion *entangled* inside the same phase.
- IP is different from the *differential VLBI* that was used to accurately tie the lunar and spacecraft orbit to the nearly inertial quasar reference frame (Ichikawa, 2003; Slade et al., 1977), which requires that single antennas at each end of the baseline move back and forth simultaneously between the two celestial sources to determine a differential phase. IP observes the sum of the fields from refer-

ence and target at each receiver, because by working with an overall signal, IP does not require to resolve the pair under study.
- IP bears some similarities with the technique of the radio pulsar timing, where the curvature of the wavefront as it reaches the Solar System causes measurable displacements in the pulse timing, along different positions of the Earth in its orbit around the Sun (Kuz'min and Kuz'min, 1988). The pulsar timing technique relies on the pulsar objects family and exploits the periodicity of their signals features, while IP makes use of a background reference object and its applicability is generalized to any class of objects.

3. Why a spacecraft is ideal

An ideal test-system for observing the IP effect should have the following basic requirements:

- A system with a high signal to noise ratio (SNR);
- A system where the distance to the source is well known;
- A system with a clearly detectable parallax phase;
- A system that behaves like a point-like source;
- An angularly close pair of objects.

We suggest that observing a spacecraft in conjunction with a distant radio source is an ideal test bench for a verification of the IP capabilities. The distance of the spacecraft can indeed be determined with a high level of precision using precise ephemerides and light travel time between the spacecraft and Earth stations, providing an accurate term of comparison for the assessment of the IP output. In addition, observing an object inside the Solar System maximizes the relative size of the parallax phase: the median rate of accumulation with time of the parallax phase (based on Eq. (8)) during the conjunctions of interest is $d\phi^{parallax}/dt \sim 0.15, 0.05, 0.67$ and 0.06°/min for Cassini, Juno, Dawn and New Horizons respectively. Both the background source and the target must be point-like sources to the interferometer: this guarantees a reliable phase estimation of both the components avoiding additional phases coming from resolved objects. There are sources that look point-like sources at km-scale baselines while they show some extended features when observed under hundreds or thousand-km-scale. To setup a solid observation, the search of the conjunctions is limited to unresolved point-like sources over 1–10 km baseline; for this purpose the use of a VLBA or VLBI calibrator source would represent the best solution. The apparent angular diameter of the spacecraft (see discussion below) guarantees that it is always unresolved by the array. Another important aspect of IP observation that requires the use of point-like sources is related to the coherence area of the latter. All the sources in fact, project a coherence area, as illustrated in Fig. 5, which depends on their apparent angular diameter; the smaller the apparent angular diameter of the source the larger is the projected area.

The correlations between two detectors are meaningful only if they are both inside the intersection of the areas of coherence of the sources. The 4-meter Cassini antenna seen at ~10 AU subtends an angle $\theta \sim 5.5 \times 10^{-7}$ arcsec, that at $\lambda = 3.6$ cm (X band) creates a coherence area of diameter $D \sim 2.6 \times 10^7$ km. Given a quasar for the background radio source with a core physical size of order 1 AU, implies an angular extent $\theta_q \sim 10^{-9}$ arcsec, which translates to an area of coherence of comparable size $D_q \sim 2 \times 10^6$ km. For the current scenario, a compact configuration with km-scale baseline Δx_{12} is blind to the effects

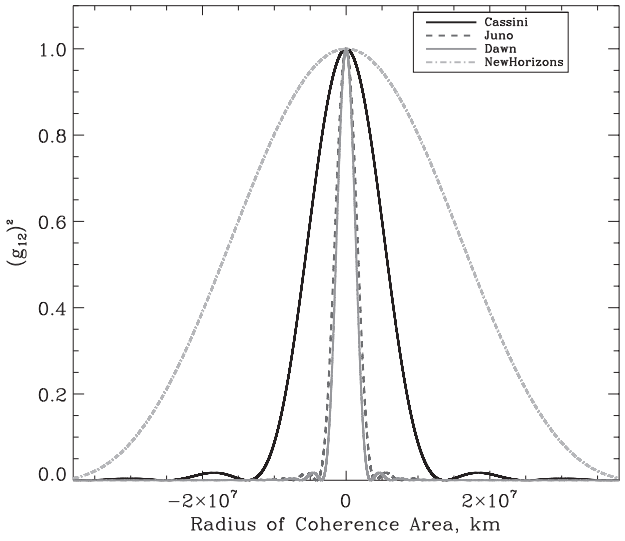

Fig. 5. The spacecraft antenna produces a zone of coherence around the observer approximately determined by a first order Bessel function. An analogous pattern is associated with the background radio source. Symbol $(g_{12})^2$ is the square of the spatial degree of coherence.

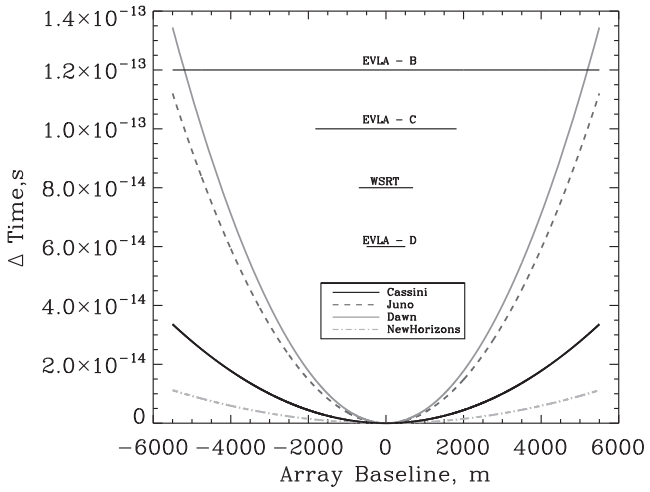

Fig. 6. Km-scale arrays like the Expanded Very Large Array (EVLA) configurations and the Westerbork array (WSRT) at $\lambda = 3.6$ cm cannot resolve the curvature of the wavefront emitted by the spacecraft with a single measurement assuming a receiver clock resolution of 10^{-12} s.

of curvature of the spacecraft wavefront within a single measurement (Fig. 6). This could be no longer true for large baselines of VLBI over which the signals of wavefronts curvature are expected to manifest with decorrelation effects already in a single observation (Fig. 7). The dimensioning of the baseline interferometer is important in order to avoid resolving the spacecraft wavefront curvature already at the first observation epoch. To demonstrate that IP can estimate the distance of the object relying on a curvature measurement that exploits a parallax effect, the sagitta of the spacecraft wavefront at the ground should lead to a signal delay between the antennas smaller than about 10^{-12} s (assuming a picosecond resolution of the receiver clock). The experiment can involve an active participation of the spacecraft or can be done in a serendipity mode during a downlink of the onboard telemetry system.

4. Simulations and estimates in detail

A simulation tool has been implemented in Matlab, in order to test and validate the described concepts and model. The average values of the parameters over the simulated observation are summarized in Table 1.

The reference frame adopted for the simulations is similar to the J2000 (inertial, centered in the center of mass of the Earth), centered instead in the center of mass of the Sun and aligned to the J2000. The motion of the Earth and of the other planets is propagated in time by using the JPL Planetary Ephemerides (Nasa website for spacecraft ephemerides) where the ephemerides are saved as files of Chebyshev polynomials fit to the Cartesian positions and velocities of the planets, Sun, and Moon. The rotation of the Earth is considered to be constant, with a period equal to one sidereal day. These solutions allow for higher accuracy in the positioning of the celestial bodies and also do not require the integration of the orbital dynamics. This

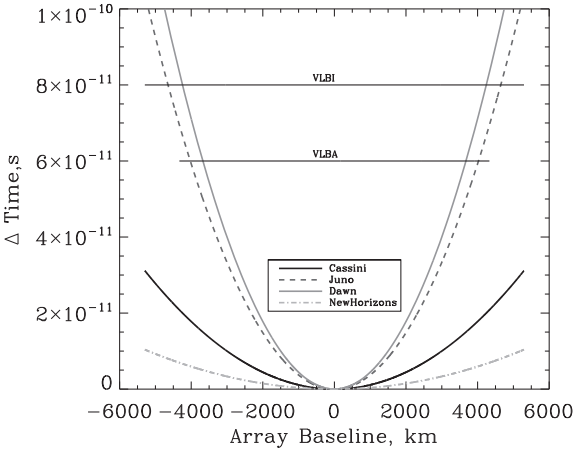

Fig. 7. With VLBA and VLBI observations at the largest baselines ($\Delta x \sim 10^3 - 10^4$ km) at $\lambda = 3.6$ cm, the effects of wavefront curvature arise already within a single measurement. Observations with these large facilities are preferred for extra Solar System objects.

Table 1
Average parameters over the course of the simulation with the Cassini spacecraft.

Parameter	Symbol	Value
Array baseline	Δx_{12}	1 km
Orbital baseline	ΔX_{12}	$\sim 10^5$ km
Cassini distance	r	~10 AU
Wavelength	λ (X band)	3.6 cm

tool allows to simulate the reciprocal positions of the spacecraft and the outer planets (e.g. see Fig. 8) and checking the visibility of the background source against possible occultations by the planets. In addition, the closest conjunctions benefit from an accurate orbital model that shall take into account the relativistic gravitational bending of the radio signals by the Solar System massive bodies (e.g. Sun, Jupiter and Saturn) (Sovers et al., 1998).

The proper motion of the spacecraft is also taken into account in the study, as provided by NASA Horizons System (Nasa website for spacecraft ephemerides). The simulator provides the estimated values for the projected ground and orbital baselines (Δx and ΔX) accounting for the orientation effects of the unit vector $\hat{\Delta x}_{12}$ relative to the sources and the unit vector $\hat{X}_{12}$. Yet $\Delta\phi^0$ will go to zero as the receiver pair separation rotates through a plane perpendicular to the vector $(\hat{r} - \hat{r}')$ while the parallax phase will remain finite.

4.1. Ideal vs real receivers

A basic and simple signature of the interferometric parallax comes from the time dependence of 2-points correlations. In general we expect a time sequence characterized by a small contribution due to the parallax phase (which grows relatively slowly with ΔX_{12}), and a dominant contribution coming from faster varying overall and VCZ phases. The equation:

$$\langle E_1 E_2^* \rangle = I_s \Lambda_s cos(\psi) + I'_s \Lambda'_s cos(\psi + \phi_{12}^{tot}) \quad (9)$$

represents the cross-correlation of the signals from two receiving systems at a single epoch. The relative phases ϕ_{12}^{tot} is the sum of the VCZ (2) and the parallax phase (3) and ψ is the fast time varying overall phase (4). This quantity is the cross-correlation output from two *ideal* receivers, noiseless and with null integration time. We assume that the intensity of the spacecraft signal is $I_s\Lambda_s = 10$ and the background radio source is $I'_s\Lambda'_s = 1$. The mathematical step-by-step derivation of this expression can be found in Appendix A. We envisage two techniques that can lead to detect IP phase signature in the signal pattern: cross-correlation of the signals and matched-filter correlations. In the direct cross-correlation, the signal from the first receiver is retrieved and cross-correlated with that coming from the second one; the observation is repeated after a given time. The effect of the $\Delta\phi_{12}^{parallax}$ term can be considered as an additional geometrical delay between the recei-

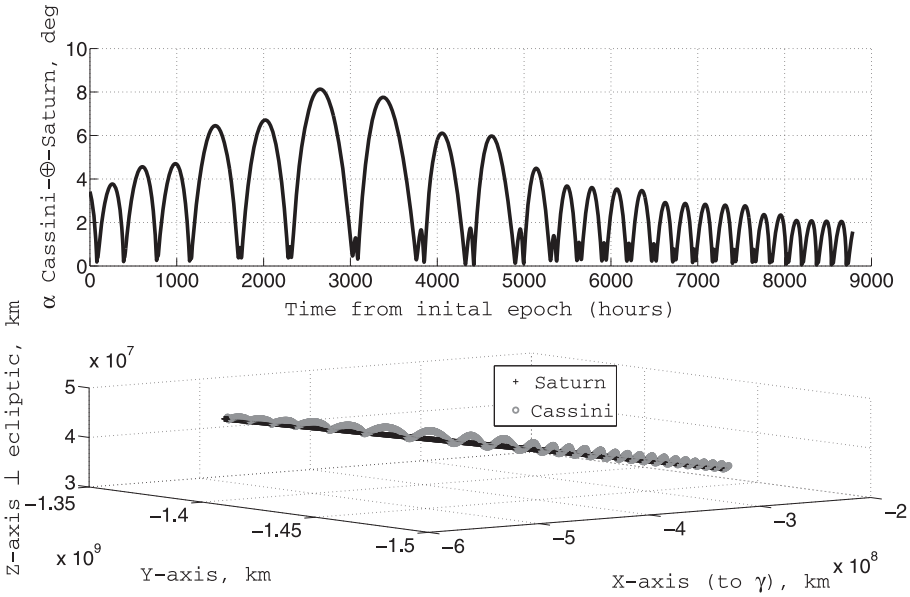

Fig. 8. Top: angle between Cassini-Earth-Saturn simulated using the JPL Planetary Ephemerides and used to estimate the angular separation between the spacecraft and the planet and finding possible occultations of the background source. Bottom: 3-D view from the simulator of the orbits of Cassini around Saturn as seen in a reference frame located in the center of mass of the Sun with the X-axis pointing towards the γ point, the z-axis normal to the to ecliptical plane and the Y-axis to complete the triad.

vers, variable with time in a way that is quasi-symmetric with respect to the spacecraft culmination on sky i.e. with respect to its passage at the meridian. This geometric delay between the two receivers that are correlating signals at equal time is observed before the culmination associated to receiver 1 and after the culmination to receiver 2. The signal patterns from the two epochs are compared and a relative phase inversely proportional to the object distance is estimated. Other indications of IP in the signal could be retrieved by using the matched filters that find the correlations between a given function (the template function described by Eq. (9)) and the measured signal pattern. Matched filter techniques have known dependence on additive stochastic noise.

When dealing with real receivers all the signals are convolved, filtered and averaged in time. The output of a correlator of a radio interferometer is called *fringe function*. In a two-element interferometer, the fringe function varies proportionally to $v\tau_g$, where $\tau_g = (\Delta x_{12}/c)\sin(\theta)$, is the geometric delay between the two antennae depending on the zenith angle θ of the pair. As the Earth rotates the most rapid rate of variation of θ is equal to the Earth's rotational velocity $\omega_\oplus \sim 10^{-4}$ rad s^{-1}. The rate of variation of $v\tau_g$ is about 10^6 times smaller than vt, and the most rapidly varying terms are filtered out by the correlator. For this reason the fast time-varying overall phase ψ cannot be tracked by the correlator. The slow time-varying phases $\Delta\phi_{12}$ and $\Delta\phi_{12}^{parallax}$ conversely contribute to the fringe function. The ordinary fringe function, standard output of an interferometer multiplier:

$$F = 2\sin(2\pi\nu t)\cdot\sin 2\pi\nu(t-\tau_g)$$

can be modified to include the *extra delay* term due to the parallax phase as follows:

$$F = 2\sin(2\pi\nu t)\cdot\sin 2\pi\nu(t-\tau_g-\tau_{parallax}) \sim \cos 2\pi\nu(\tau_g+\tau_{parallax}) \quad (10)$$

with the terms $2\pi\nu\cdot\tau_{parallax} = \Delta\phi_{12}^{parallax}$ and $2\pi\nu\cdot\tau_g = \Delta\phi_{12}$ corresponding to:

$$\Delta\phi_{12}^{parallax} \sim \frac{\Delta x_{12}\cdot\Delta X_{12}}{r\lambda} \qquad \Delta\phi_{12} \sim \frac{\Delta x_{12}\cdot\sin\theta}{\lambda} \quad (11)$$

taking into account the effect of the bandwidth we get the so called *fringe washing function*:

$$F(\tau_g) = \exp\left[-2\left(\frac{\pi\Delta x_{12}\Delta\nu\sin\theta}{c}\right)^2\right]\cos 2\pi\nu(\tau_g + \tau_{parallax})(V_{array})^2 \quad (12)$$

with $\Delta\nu$ bandwidth of observation and V_{array} overall signal intensity in input to the radio receiver. The effect of the parallax phase on the fringe pattern can be observed in Fig. 9 where also the time dependence of the phases is shown.

By observing the pair at two different epochs at the opposite sides of its culmination path we look for two time windows in which the array projected baselines (Δx) are the same in modulus and the relative geometric phases $\Delta\phi_{12}(t_1)$ and $\Delta\phi_{12}(t_2)$ give the same delay contribution. In this condition the relative shift in the fringe patterns at the two epochs is addressed almost entirely to the parallax phase term as shown in Fig. 10. With this geometry possible inequalities of $\Delta\phi_{12}$ between the epochs could originate from the object proper motion. In this specific simulation we compare the amplitude signals correlation patterns

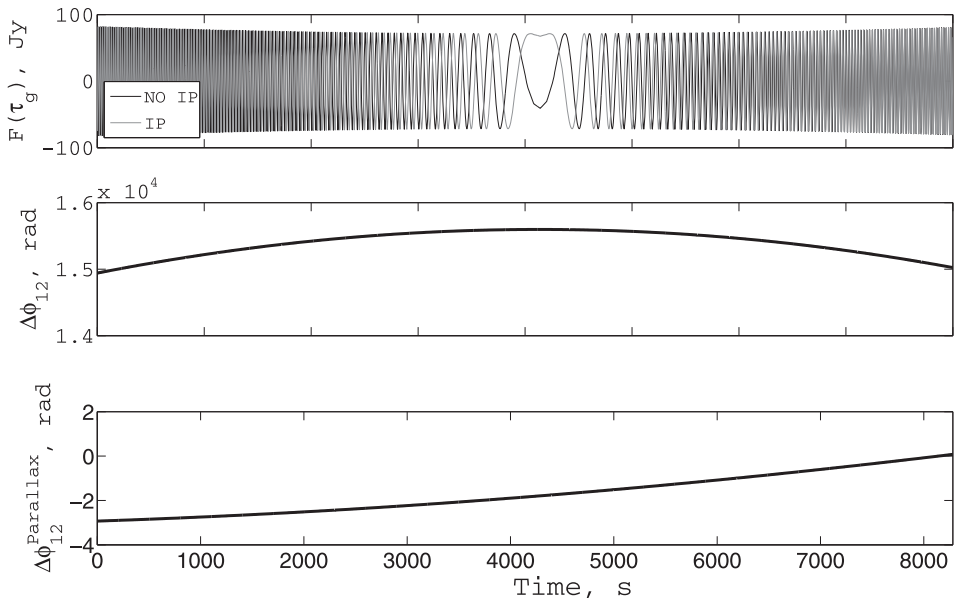

Fig. 9. Phases simulation for Cassini spacecraft culmination in sky as seen from a mid-latitude site (e.g. VLA Observatory). **Top**: Fringe washing function $F(\tau_g)$ with (gray line) and without (black line) parallax term for an overall input signal $S = 10$ Jy and a bandwidth $\Delta v = 1$ MHz. **Middle**: geometric phase $\Delta\phi_{12}$ due to τ_g. **Bottom**: parallax phase $\Delta\phi_{12}^{parallax}$. $\Delta\phi_{12}$ grows and decreases symmetrically with time in absence of object proper motion, while the parallax phase increases due to the orbital baseline. Over longer time intervals the modulation on $\Delta\phi_{12}^{parallax}$ by the ground baseline is also observable. Evident signals of IP phase are detectable over an interval of about 2 h (bottom panel).

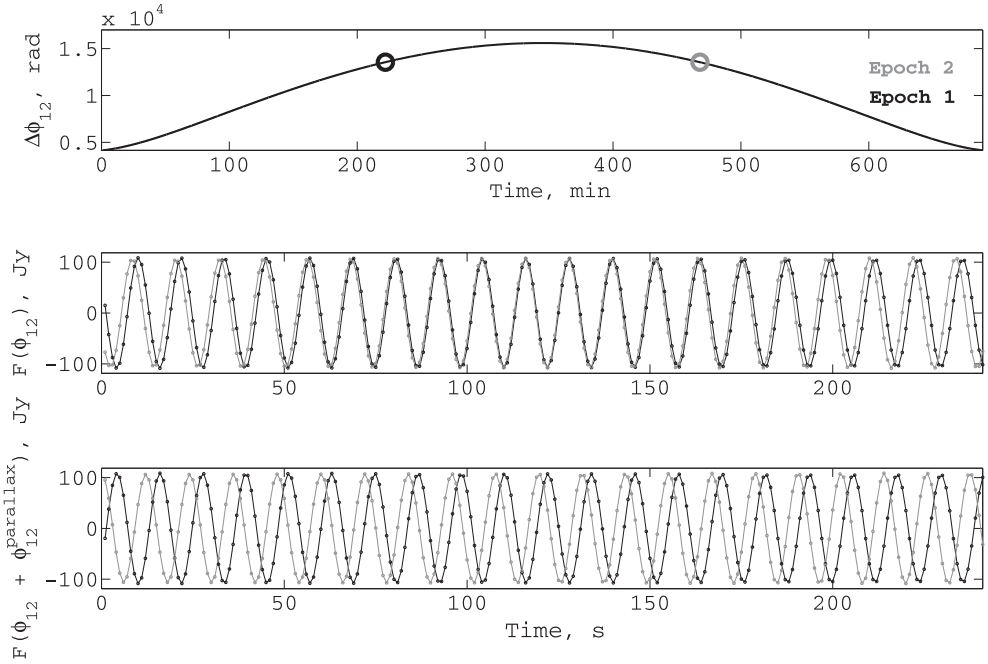

Fig. 10. **Top:** Two observations are performed at two different epochs (1 (black) and 2 (gray)) separated by ~6 h. ϕ_{12}^0 is continuously varying with time, increasing during first epoch and decreasing during the second epoch. **Middle:** fringe function signal stream for six minutes of observation; an optimal window of observation exists in which the contribution from the geometric phases $\phi_{12}(t_1)$ and $\phi_{12}(t_2)$ is the same and the relative shift among the fringe patterns is minimum. **Bottom:** taking into account $\phi_{12}^{parallax}$ in the same time frame, a substantial relative shift (related to target object distance) between the fringe patterns originates. The measurement of this relative phase shift leads to an estimation of the target object distance (Eq. (6)).

between two epochs of observation (top plot Fig. 10), six minutes each, separated by a six-hour time interval (middle and bottom plots Fig. 10) around a spacecraft culmination in sky. We retrieve a best distance estimation for Cassini $r \sim 9.6$ AU that is only 5% different from the value foreseen by the ephemerides. This important result has to be weighted with the different sources of error affecting the measured phase (Thompson et al., 2004):

$$\phi_{meas} = \phi_{vis} + \phi_{inst} + \phi_{pos} + \phi_{ant} + \phi_{atmos} + \phi_{ionos} \quad (13)$$

ϕ_{meas} is the overall sum of respectively the phase due to the source visibility, instrumental effects, errors due to the assumed source and antenna positions, the effect of the neutral atmosphere (Troposphere) and of the Ionosphere. The visibility phase ϕ_{vis} is associated to the geometric features of the source and it is zero for a point-like source as assumed in our scenario; the instrumental ϕ_{inst} includes clock instabilities and receiver noise (electronics and thermal) that do not represent a particular issue, e.g. a high frequency Gaussian noise from the electronics is highly variable in time and it is removed by the correlator and filters while other instrumental instabilities can be calibrated observing strong sources a few times per day (Reid and Honma, 2014). ϕ_{pos} represents the error in the assumed source position while $\phi_{ant} \sim |\delta\Delta x|/c$ is the phase due to the antenna position error. ϕ_{ant} is estimated through geodetic VLBI and GPS measurements that lead to locate the antenna position with an accuracy of ~3 mm; the gravity flexures at different pointing directions are quasi-static contributions that can be corrected using lookup tables or opto-mechanical models of the antenna. Including in ϕ_{ant} also possible variations in the Earth's rotation rate, this phase has a smaller impact than the uncertainty in atmospheric propagation delays (Reid and Honma, 2014). The dominant phase error is then represented by the atmospheric perturbation $\phi_{atmos} + \phi_{ionos}$ that is split into tropospheric and ionospheric perturbations depending on the observing wavelength. At $\nu = 8$ GHz the phase error due to the tropospheric perturbation under stable conditions is around 5° over a baseline of ~1 km (Gary, 2014) and standard measurements conducted with VLBA and VLBI systems with periodic switching to a calibrator source show a phase stability of a few degrees (~< 10°) within observation runs of 8 h (Beasey and Conway, 1995). At $\nu = 22$ GHz with VLA baselines between 1 and 20 km Carilli and Holdaway (1999) demonstrated that fast phase switching can reduce the RMS atmospheric phase stably down to 5° over periods of ~20 s. Any time-varying phase induced by the atmosphere creates a bias in the distance estimation because the atmospheric phase behaves indistinguishably from the geometrical time delay τ_g and the parallax term (fringe function is modified to $F \sim \cos 2\pi\nu(\tau_g + \tau_{parallax} + \tau_{atmosphere})$). In the specific case of Cassini, for the simulation scenario assessed, a gross error of 5° due to the atmospheric phase would lead to an error of about 1 AU in the distance estimation that corresponds to a 10% uncertainty in the measurement. As in standard image production with aperture synthesis, also in the IP scheme, ϕ_{meas} is corrected with the phase referencing technique observing alternatively the target and a nearby calibrator with periods of a few minutes each to interpolate the phase without ambiguities and with limited errors. The phase calibrator must be an unresolved, bright source with known position and it should fall within the isoplanatic angle so that the differences between the two objects in the atmospheric terms can be neglected. If phase referencing is performed correctly, the corrected phase of the target is reduced to (Thompson et al., 2004):

$$\phi^t - \hat{\phi}^c = \phi^t_{vis} + (\phi^t_{pos} + \hat{\phi}^c_{pos}) \quad (14)$$

where t and c indices refer to target and calibrator and the $\hat{\phi}$ indicates the interpolated value of the phase. Since the target is a point-like source $\phi^t_{vis} = 0$ (see Section 3), Eq. (14) turns out to depend only on the relative positions of the two sources. The last term that the IP observation should care about is the w-term in the visibility function associated to the target and the background source. In standard interferometry a right-handed coordinate system (u, v, w) is assumed, with the (u, v) plane normal to the direction of photon propagation w and of the phase center reference position $\mathbf{s}_0$. In such a system the baseline has a component $\Delta\mathbf{x}_{12}\sin(\theta)$ in the direction of the phase center, $\mathbf{s}_0$, and $w = \Delta\mathbf{x}_{12} \cdot \mathbf{s}_0$ that mimics the *delay* arising from the curvature of the wavefront. This curvature delay is delicate to model and it is challenged by all the phase errors discussed above. For this reason, the selection of a point-like object ($\phi_{vis} = 0$) as background source is mandatory. In a coordinate system (l, m) corresponding to the projection of the celestial sphere onto a plane tangent to the field center, the coordinates of a point are proportional to the sine of the corresponding angles in sky. In such a coordinate system, the geometric time delays between a two-elements interferometer associated to the two point-like sources (target and reference) reduce to $\pi w(l_i^2 + m_i^2)$, where l_i and m_i are the direction cosines of the point sources with respect to the phase center $\mathbf{s}_0$. In this latter case where both the target and the background source are point-like sources the geometrical delay model drastically simplifies the measurement leading to a reliable observational scenario for IP.

4.2. Perspectives for astronomy

The pathfinder experiment we propose in this paper has the goal of assessing the reliability of the IP measurement on typical Solar System distance scales. The extension of this technique to outer distance scales requires the development of a dedicated project and new technological challenges. Nevertheless if the latter achievements will be fulfilled, IP opens new perspectives for Astronomy both in the radio and optical domains. At radio wavelengths, the distance of pulsars and masers could be measured against a background of extragalactic objects, or a nearby extragalactic radio source could be measured against a powerful radio source at cosmological distances. The future major radio telescopes arrays, the Square Kilometer Array (SKA) and the Event Horizon Telescope, thanks to their unprecedented sensitivity, phase stability and resolution (Fomalont and Reid, 2004; Fish, 2010) will provide a powerful tool and attractive perspectives for galactic and extragalactic objects, pushing forward the limit of

the current instrumentation and leading to increase the technological readiness level of certain techniques that may contribute to the development of IP scenarios. The SDSS Quasar Catalog (Schneider et al., 2007) reports about 346 close pairs of quasars that are apparent superpositions because they show radically different redshifts and the brightest pairs (radio-loud objects) would be suitable targets for the IP technique. One % (3 pairs) of this sample are made of two bright radio sources closer than 1 arcmin, and in the third release of the Large Quasar Astrometric Catalog (Souchay et al., 2015) other 7 pairs of quasars are found to fit the IP requirements. The current limitation of the amplitude interferometry is that it requires extremely precise phase referencing, it is inherently limited by the atmospheric perturbations at a ~degree level and this latter disturbance increases with the array baseline. A complementary scenario, barely sensitive to atmospheric perturbations, involves the use of the Intensity Interferometry (II); this technique was pioneered in Astronomy thanks to the work of Hanbury-Brown and Twiss at the Narrabri Observatory in the decades of sixties and seventies (Hanbury Brown and Twiss, 1958). An intensity interferometer measures the second-order coherence of the light by observing the correlation in the time of arrival of photons at different telescopes in space. The telescopes are not optically linked like in the amplitude-phase interferometry. The light signals are digitized and the correlations are done by software and electronics that provide a time resolution of a few nanoseconds. For this reason optical paths differences in the order of $\tau_{electronics}c \sim 0.3$ m can be tolerated, leading this technique to be relatively insensitive to atmospheric perturbations and other systematic and random errors that limit the amplitude optical interferometry beyond 0.3 km-scale baselines. Although this technique is disfavored in terms of SNR with respect to the amplitude interferometry, the next generation of imaging air Cherenkov telescopes (e.g. CTA) will provide a huge light collecting power and baselines at km-scale. Cherenkov telescopes have large point spread functions (e.g. 5–10 arcmin) that fulfill the requirement of observing the overall electric field from the pair. The tolerable phasing errors of II (~0.3 m for time resolution of ~1 ns) make feasible the realization of a km-scale array at optical wavelengths that has comparable angular resolution with the VLBI system at radio frequencies: working with a ground baseline $\Delta x = 1$ km at $\lambda = 0.4 - 0.5$ μm is equivalent to a VLBI baseline $\Delta x = 1e4$ km at $\lambda = 1$ cm. A couple of 24 m Cherenkov telescopes should reach a limiting magnitude in B band $m_B \sim$ 10–11 for 10 h of observation, that could be enhanced by adding more telescopes to the interferometer or more channels per telescope. Assuming $m_B \sim$ 10–11 as limiting magnitude for the faintest detectable sources (SNR ~ 5) many objects could be the target for IP measurements. Inside the Milky Way, at optical wavelengths, many galactic stellar objects could be targets for IP measurements. For example, foreground galactic field stars could be measured against background star cluster members, or at the opposite, a member of a foreground star cluster could be referenced to a background field star. From the study of stellar proper motions and radial velocities (Nardiello, 2016; Geller et al., 2015), the cluster membership probabilities for a certain source can be estimated, and once the two populations (cluster and field) are separated, the cluster members can be referenced to the stars field in the IP scheme. Open clusters like M67 (Nardiello, 2016), the Pleiades (Sarro, 2014) and NGC 4755 (Corti and Orellana, 2013) are only some examples of possible clusters hosting objects hot and bright enough for II and with detailed memberships studies. Also the supernovae, even if transient events, could be interesting point-like, background sources readily detectable at Mpc-scale thanks to their high luminosity during the first month around the light curve maximum ($M_B \sim -17$ assuming SN Ia).

5. Conclusions

We have described an experimental scenario to evaluate the performances and potentialities of a new method to estimate the geometric distance of the astronomical sources. The experiment can be performed with state-of-the-art technology. A pathfinder simulation based study with the Cassini spacecraft has been carried out to develop an observation that maximizes the interferometric parallax effects. The results indicate that IP signals leading to a reliable distance estimation (uncertainties ~5–10%) are obtainable already within a limited time frame (~2–6 h) and in the presence of atmospheric phase perturbations. The spacecraft observation can be done also in a serendipity mode during a downlink of the onboard telemetry system. The proposed experiment is an assessment observation of a novel concept and as any first attempt measurement, there might be some details that can be fully understood and consolidated only with a test-on-sky of the scenario modeled with the hereby simulations. The proposed test-experiment does not seek to reproduce the high accuracy of classical trigonometric parallax, image-based, measurements by VLBA and VLBI. Rather, it indicates that IP is conceptually new and uses much simpler phase information, not requiring image formation nor target resolution in the pair. In the perspective of the new generation observatories such as SKA at radio frequencies and CTA at optical wavelengths a dedicated project with future technological developments characterized by extreme phase stability, real-time phase calibration techniques and ultra-fast detectors could pave the road to new scenarios for the distance estimation of hundreds of galactic sources and beyond.

Acknowledgements

Authors are grateful to Dr. E. P. Farina, D. Jones, M. Clemens, M. Barbetta, Prof. D. Dravins, Prof. L. Iess and his team, N. Schneider, C. Sigismondi, R. McGurck and V. Guglielmo for the important discussions and com-

ments to this document. Authors acknowledge Dr. M. Rayman and G. Bellei for the information and discussions about the satellites ephemerides. The corresponding author gratefully acknowledges the suggestions of Dr. M. Pajola on spacecraft flight dynamics and of I. Baronchelli on Chebyshev polynomials. Authors are deeply grateful to the anonymous referees who contributed to the improvement of the paper.

Appendix A. In the following, the most important calculations that lead to the phases used along the paper are derived following (Jain and Ralston, 2008). The distance from the Jth detector to the source is expanded (as shown in Fig. 11):

$$r_J = r - \hat{\mathbf{r}} \cdot \mathbf{x_J} + \frac{1}{2r}\sum_{i,j=1}^{3} x_J^i \delta_T^{ij}(r) x_J^i + O(1/r^2) \tag{15}$$

where $\mathbf{r}$ and $\mathbf{x_J}$ are the position vectors of the source and the Jth detector relative to the origin. Consider the Green function for light propagation from source to detectors:

$$G_{x_J,r} = \frac{1}{4\pi}\frac{e^{ik|\mathbf{r}-\mathbf{x_J}|}}{|\mathbf{r}-\mathbf{x_J}|} \sim \frac{e^{ikr}}{4\pi r} e^{-ik\hat{\mathbf{r}}\cdot\mathbf{x_J}} \exp\left(\frac{ik}{2r}\sum_{i,j=1}^{3} x_J^i \delta_T^{ij} x_J^i\right) \tag{16}$$

we compute the two–points amplitude correlations:

$$\langle (E+E')_1 \cdot (E+E')_2^* \rangle = E_1 E_2^* + E_1 E_2'^* + E_1' E_2^* + E_1' E_2'^* \tag{17}$$

the mixed terms $E_1 E_2'^*$ and $E_1' E_2^*$ are null because the two sources are completely uncorrelated. The pre–factors $\frac{e^{ikr}}{r}, \frac{e^{ikr'}}{r'}$ are dropped off because they cancel out in calculations.

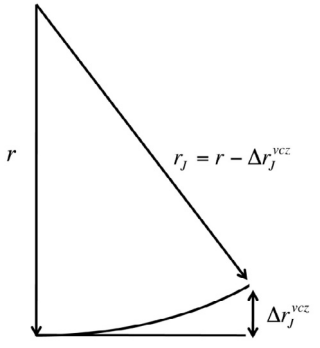

$$r_J = r - \hat{r}\cdot x_J + \frac{1}{2r}\sum_{i,j=1}^{3} x_J^i \delta_T^{ij}(r) x_J^j + O(1/r^2)$$

Fig. 11. The third term of the Taylor expansion accounts for curvature of the wavefront.

$$\langle (E+E')_1 \cdot (E+E')_2^* \rangle = \frac{1}{16\pi^2 r^2} e^{-ik\hat{\mathbf{r}}(\mathbf{x_1}-\mathbf{x_2})} \cdot e^{\frac{ik}{2r}\delta_T^{ij}(x_1^i x_1^j - x_2^i x_2^j)} + \frac{1}{16\pi^2 r'^2} e^{-ik\hat{\mathbf{r}}'(\mathbf{x_1}-\mathbf{x_2})} \cdot e^{\frac{ik}{2r'}\delta_T^{ij}(x_1^i x_1^j - x_2^i x_2^j)} \tag{18}$$

$$\langle (E+E')_1 \cdot (E+E')_2^* \rangle = e^{-ik\psi}\left[\frac{I_S}{r^2} + \frac{I_S'}{r'^2} e^{-i\phi_{12}^0 - i\phi_{12}^{parallax}}\right] \tag{19}$$

I_S and $I_{S'}$ parameterize detected source intensities, $\phi_{12}^0 = k\Delta\mathbf{x}_{12}\cdot(\hat{\mathbf{r}}-\hat{\mathbf{r}}')$ the VCZ phase, $\phi_{12}^{parallax} = -k(\frac{1}{r}-\frac{1}{r'})\Delta\mathbf{x}_{12}\cdot\delta_T\cdot\mathbf{X}_{12}$ the parallax phase and $\psi = \hat{\mathbf{r}}\cdot(\mathbf{x}_1-\mathbf{x}_2) - \sum_{i,j=1}^{3}(x_1^i x_1^j - x_2^i x_2^j)\delta_T^{ij}(\mathbf{r})/2r$ the overall phase.

References

Beasey, A.J., Conway, J.E., 1995. VLBI phase-referencing, very long baseline interferometry and the VLBA. ASP Conference Series, vol. 82.
Carilli, C.L., Holdaway, M.A., 1999. Tropospheric phase calibration in millimeter interferometry. Radio Sci. 34 (4), 817–840.
Condon, J.J., Cotton, W.D., Greisen, E.W., et al., 1998. The NRAO VLA sky survey. ApJ 115, 1693–1716.
Corti, M.A., Orellana, R.B., 2013. Members of Centaurus OB1 and NGC 4755: new spectroscopic and astrometric studies. A&A 553, A108.
de Bruijne, J.H.J., 2012. Science performance of Gaia, ESA's space-astrometry mission. Astrophys. Space Sci. 341, 31–41.
Dravins, D., LeBohec, S., Jensen, H., Nunęz, P.D., 2012. Stellar intensity interferometry: prospects for sub-milliarcsecond optical imaging. Astropart. Phys. 56, 143–167.
Fish, V., 2010. Observing event horizons with high-frequency VLBI. In: Proceedings of the 10th European VLBI Network Symposium and EVN Users Meeting: VLBI and the New Generation of Radio Arrays.
Fomalont, E., Reid, B., 2004. Microarcsecond astrometry using the SKA. New Astron. Rev. 48, 1473–1482.
Gary, D.E., 2014. Physics 728, Radio Astronomy Course. Website <https://web.njit.edu/~gary/728/>.
Geller, A.M., Latham, D.W., Mathieu, R.D., 2015. Stellar radial velocities in the old open cluster M67 (NGC 2682). I. Memberships, binaries, and kinematics. AJ 150, 97.
Hachisuka, K., Brunthaler, A.A., Menten, K.M., et al., 2006. Water maser motions in W3(OH) and a determination of its distance. ApJ 645, 337.
Hanbury Brown, R., Twiss, R.Q., 1958. Interferometry of the intensity fluctuations in light. III. Applications to astronomy. Proc. Roy. Soc. Lond. 248 (1253), 199–221.
Ichikawa, T., 2003. The application of differential VLBI to planetary approach navigation. In: SICE Annual Conference in Fukui, August 4–6.
Jain, P., Ralston, J.P., 2008. Direct determination of astronomical distances and proper motions by interferometric parallax. A&A 484, 887–895.
Jones, D.L., Fomalont, E., Dhawan, V., et al., 2011. Very long baseline array astrometric observations of the Cassini spacecraft at Saturn. ApJ 141, 29.
Kopeikin, S., Schäfer, G., 1999. Lorentz covariant theory of light propagation in gravitational fields of arbitrary-moving bodies. Phys. Rev. D 60, 124002.
Kuz'min, A.D., Kuz'min, O.A., 1988. Pulse timing as a pulsar distance probe. Sov. Astron. Lett. 14, 180.
Nardiello, D., Libralato, M., Bedin, L.R., et al., 2016. Variable stars in one open cluster within the Kepler/K2-Campaign-5 field: M 67 (NGC 2682). MNRAS 455, 2337–2344.

Nasa Website for Spacecraft Ephemerides: <http://ssd.jpl.nasa.gov/horizons.cgi>.
Perryman, M.A.C., Lindegren, L., Kovalevsky, J., et al., 1997. The HIPPARCOS catalogue. A&A 323, L49–L52.
Reid, M.J., Honma, M., 2014. Microarcsecond radio astrometry. Annu. Rev. Astron. Astrophys. 52, 339–372.
Reid, M.J., Menten, K.M., Zheng, X.W., et al., 2009. Trigonometric parallaxes of massive star-forming regions. VI. Galactic structure, fundamental parameters, and noncircular motions. ApJ 700, 137–148.
Sarro, L.M., Bouy, H., Berihuete, A., et al., 2014. Cluster membership probabilities from proper motions and multi-wavelength photometric catalogues. A&A 563, A45.
Schneider, D.P., Hall, P.B., Richards, G.T., et al., 2007. The sloan digital sky survey quasar catalog. IV. Fifth data release. ApJ 134, 102–117.
Slade, M.A., Preston, R.A., Harris, A.W., et al., 1977. ALSEP-quasar differential VLBI. The Moon 17, 133–147.
Souchay, J., Andrei, A.H., Barache, C., et al., 2015. The third release of the large quasar astrometric catalog (LQAC-3): a compilation of 321 957 objects. A&A 583, A75.
Sovers, O.J., Fanselow, J.L., Jacobs, C.S., 1998. Astrometry and geodesy with radio interferometry: experiments, models, results. Rev. Mod. Phys. 70 (October).
Thompson, A.R., Moran, J.M., Swenson Jr., G.W., 2004. Interferometry and Synthesis in Radio Astronomy, second ed. Wiley-Vch.
van Langevelde, H.J., Diamond, P.J., Vlemmings, W., et al., 1999. VLBI measurements of the parallax and proper motion of U Herculis. New Astron. Rev. 43, 575.